POLITECNICO
MILANO 1863

SCUOLA DI INGEGNERIA INDUSTRIALE
E DELL'INFORMAZIONE

Executive Summary of the Thesis

Experimental investigation of a Dy-doped fluoride fibre laser in the 3 µm wavelength emission range

Laurea Magistrale in Engineering Physics - Ingegneria Fisica

Author: Fedele Pisani

Advisor: Prof. Paolo Laporta

Co-advisor: Dr. Gianluca Galzerano

Academic year: 2021-2022

1. Introduction

The mid-infrared spectral region, usually defined as the wavelength interval $2 \div 20\,\mu m$, is where most trace gas molecules have their fundamental rovibrational absorption bands. The $3 \div 5\,\mu m$ wavelength range is of particular interest because it present relatively small water vapour absorption and contains the strongest absorption bands of molecules with CH, NH or OH stretching vibrations.

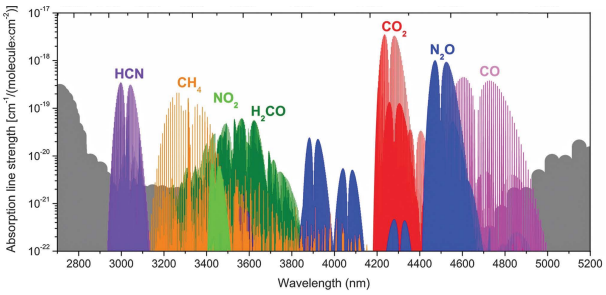

Figure 1: Absorption spectra of some trace gases in the $3 \div 5\,\mu m$ spectral region.

The aim of this thesis work is to experimentally investigate a novel fibre laser source with wide emission in the 3 µm spectral range, which can find interesting application in broadband molecular spectroscopy. To this purpose, the Dy-doped fluorozirconate fibre was selected as active medium for its wavelength emission tuneability in the range from 2.9 µm to 3.2 µm. In particular, we have investigated the laser performance of this in-band pumped fibre both in a CW configuration and in passive Q-switching regime. Continuous wave laser operation was investigated for output coupling from 10 % to 50 %, leading to a maximum laser output power of 248 mW and a maximum slope efficiency from absorbed pump power to output power of 44 %. Passive Q-switching laser operation was achieved with multiple choices of saturable absorber, demonstrating stable operation with a minimum pulse duration of 464 ns, a highest repetition frequency of 210 kHz and peak pulse powers up to 3069 mW.

2. Experimental setups and results

2.1. Active medium

The active medium of our configurations is the Dy-doped ZBLAN fibre described in Table 1. ZBLAN, a fluorozirconate glass, was specifically chosen as host material for its low attenuation up to 5 µm and low maximum phonon energy.

Core diameter	d_{core}	12.5 µm
Cladding diameter	d_{clad}	125 µm
Numerical aperture	NA	0.16
Refractive index	n	1.49
Cut-off wavelength	λ_{co}	2.55 µm
Doping concentration	N_0	3.63×10^{25} m^{-3}
Length	L	1.82 m
Max phonon energy	$\hbar\omega_{ph}$	590 cm^{-1}

Table 1: Dy^{3+}:ZBLAN fibre specifications.

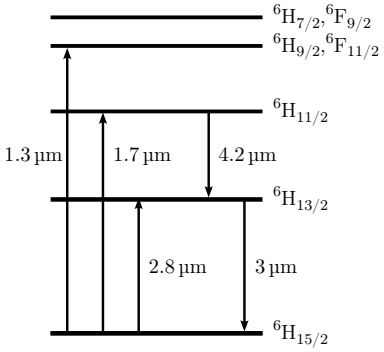

Figure 2: Energy levels of the Dy ion in ZBLAN.

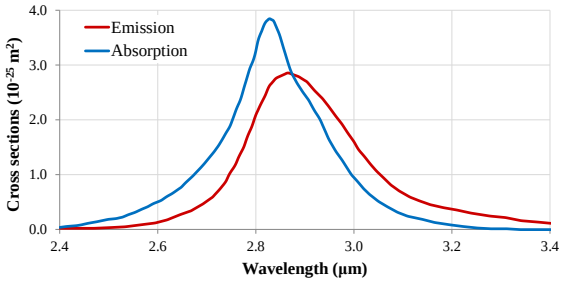

Figure 3: Absorption and emission cross-sections of the Dy^{3+}:ZBLAN fibre.

The fibre core is doped with Dy^{3+} ions, whose relevant energy levels are shown in Figure 2. We exploit the $^6H_{15/2} \leftrightarrow {}^6H_{13/2}$ transition, whose absorption and emission spectra are reported in Figure 3, at which the dysprosium ion acts as a quasi-three level laser system, allowing in-band pumping with very high quantum efficiency. Moreover, the large emission cross-section of Dy allows wide wavelength tuning in continuous wave and short pulse duration in Q-switching and mode-locking. Finally, Dy can show laser action up to 3.2 µm, where other rare earths have no emission.

2.2. Pumping scheme

The Dy^{3+}:ZBLAN active fibre was pumped in-band with a continuous wave diode-pumped Er^{3+}:ZBLAN fibre laser emitting at 2825 nm. The pump power injected into a Dy-doped fluoride fibre is limited by thermal issues and the risk of damaging the fibre end-face. To increase the maximum injected pump power by up to a factor of two, we designed a pumping scheme where the fibre is pumped from both sides, as shown in Figure 4.

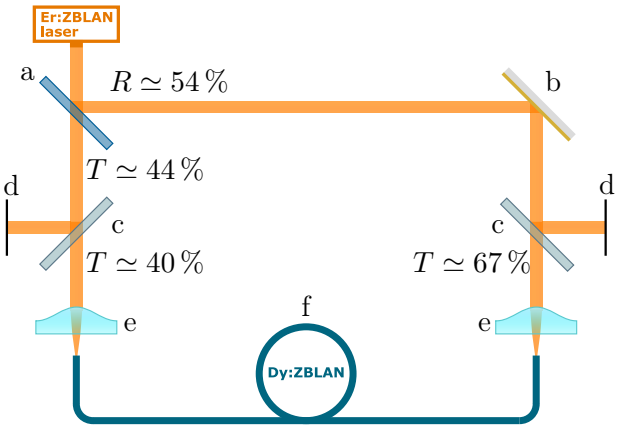

Figure 4: Pumping scheme: a) beam splitter; b) gold mirror; c) dichroic mirrors; d) beam stoppers; e) ZnSe aspheric lenses; f) Dy:ZBLAN fibre.

Our measurements show that 24 % of the power emitted by the Er^{3+}:ZBLAN pump laser reaches the left tip, while 27 % reaches the right tip. The maximum power at which the pump laser can be safely operated is thus determined by the risk of damaging the right fibre tip. The maximum total power that can be coupled into the fibre is therefore 0.24/0.27 = 86 % larger than with single-side pumping. Moreover, this improvement can be combined with the one given by other fibre protection techniques, such as fibre cladding mode strippers and InF_3 fibre end caps. Given the very small core diameter (12.5 µm), precise and stable positioning of the fibre tips was of great importance. In the initial configuration, the fibre tips were placed on three-axis stages using tapered v-groove fibre holders. Since the quality of the fibre tips was a major constraint, we later decided to use ferrules, which make it possible to improve cuts by polishing the fibre end-faces. The ferrules were placed on three-axis stages using strain relief clamps.

Figure 5 shows that the tips mounted with ferrules, which have been polished, have better performance.

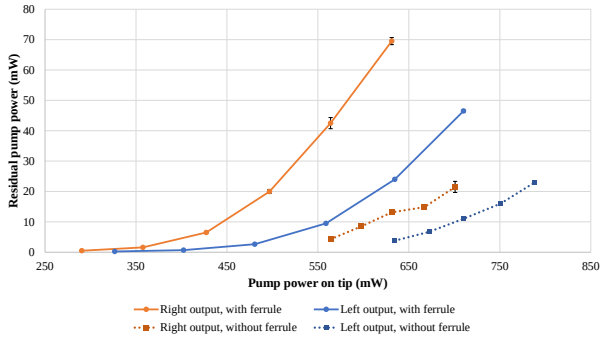

Figure 5: Residual pump power measured at the output of the fibre as a function of the power measured just before the other end.

2.3. Continuous wave setup

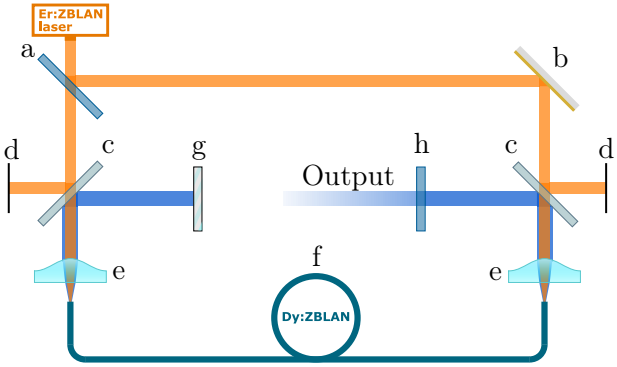

Figure 6: Linear resonator design for continuous wave operation: a-f) see Figure 4; g) back-reflecting mirror; h) output coupler.

Figure 6 shows the linear resonator design used to achieve continuous wave operation. On the left, the laser cavity is closed by a dielectric mirror with $R = 98\,\%$, while on the right we tested different sapphire output couplers. Figure 7 reports as a function of the provided pump power the measured laser output power and the corresponding linear fitting, from which the slope efficiencies and threshold pump powers were estimated.
From the theory, the slope efficiency is expected to be

$$\eta = \eta_0 \frac{\gamma_2}{\gamma_1 + \gamma_2 + 2\gamma_i} \simeq \eta_0 \frac{\gamma_2}{\gamma_2 + 2\gamma_i}$$

where $\gamma_2 = -\ln(1 - T_{OC})$ are the logarithmic losses of the output coupler, $2\gamma_i$ are the round-trip logarithmic internal losses of the cavity and $\gamma_1 \simeq 0$ are the logarithmic losses of the dielectric mirror. We used this analytical model to fit the slope efficiencies computed with respect to the power absorbed by the fibre. The estimate of the round-trip logarithmic internal losses is $2\gamma_i \simeq 0.30$, while the estimate of the maximum slope efficiency is $\eta_0 = 0.60$. This value is lower than the expected one, 0.83, computed considering the in-band quantum efficiency and the spatial overlap between the pump and laser beams.

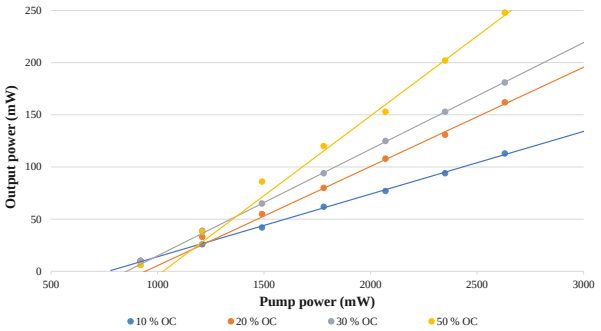

Figure 7: Laser output power when the cavity is closed by the dielectric mirror, for different output couplers.

Multiple continuous wave measurements were later performed with the 20 % output coupler to test different back-reflecting mirrors. Figure 8 reports these measurement and the linear fitting performed on them, from which the slope efficiencies and threshold pump powers were estimated. The measurements with the protected gold mirror coated with a graphene monolayer and the ones with the mid-infrared enhanced gold mirror correspond to polished fibre tips, which allow better coupling. We see that the graphene-coated mirror has better performance than the other one, but both gold mirrors perform worse than the dielectric mirror.

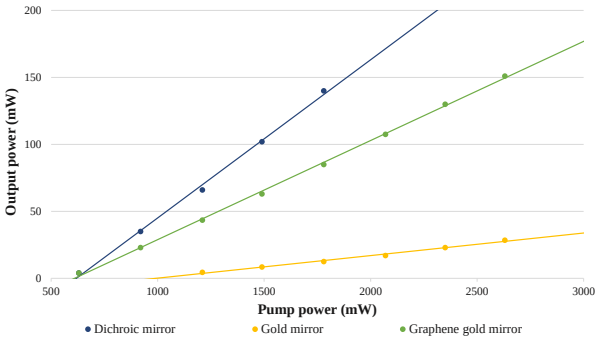

Figure 8: Laser output power for different back-reflecting mirrors, using a 20 % output coupler.

2.4. Pulsed setup

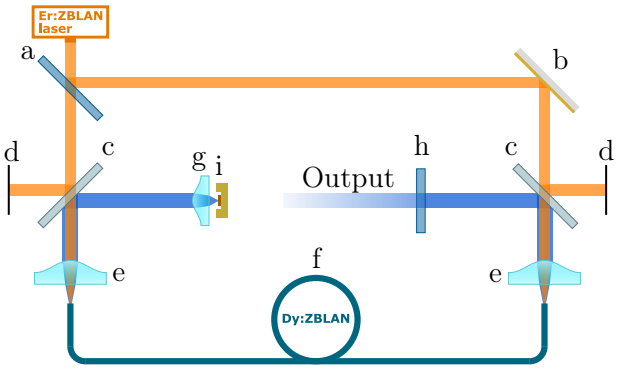

Figure 9: Linear resonator design for pulsed operation: a-i) see Figure 4; l) CaF_2 plano-convex lens; m) output coupler; n) saturable absorber mirror.

As shown in Figure 9, to achieve pulsed operation we substituted the back-reflecting mirror with a $f = 20\,\text{mm}$ CaF_2 plano-convex lens followed by a saturable absorber mirror. We investigated multiple combinations of output couplers and saturable absorbers, starting from a semiconductor one, the SAM-3000. As shown in Figure 10, the laser operated in Q-switching regime. The full width at half maximum $\Delta\tau$, repetition frequency f_R and average power P_{avg} were measured, while the peak pulse power was computed as $P_{\text{peak}} \simeq 0.94 P_{\text{avg}}/(f_R \Delta\tau)$.

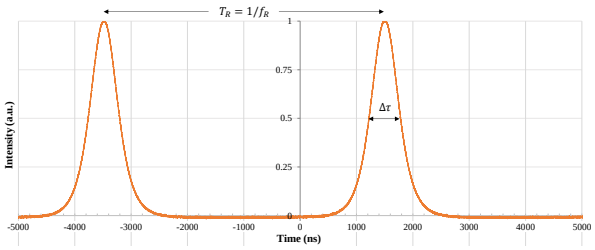

Figure 10: Example of oscilloscope output with the SAM-3000.

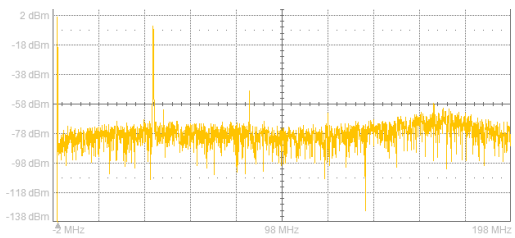

Figure 11: Example of fast Fourier transform with the SAM-3000.

As shown in Figure 11, the fast Fourier transform of the measured signal presents a strong peak at 42 MHz and a weaker one at double the frequency. Since the frequency of the main peak corresponds to the free spectral range, estimated as $\text{FSR} = 1/T = c/[2(n_{\text{fibre}} l_{\text{fibre}} + l_{\text{air}})]$, the two peaks represent mode beating between very close longitudinal modes of the cavity. This spectrum corresponds therefore to Q-switching with only a few modes oscillating in the cavity. This situation is far from optimal for achieving mode-locking, which requires a very high number of modes to be oscillating in the cavity.

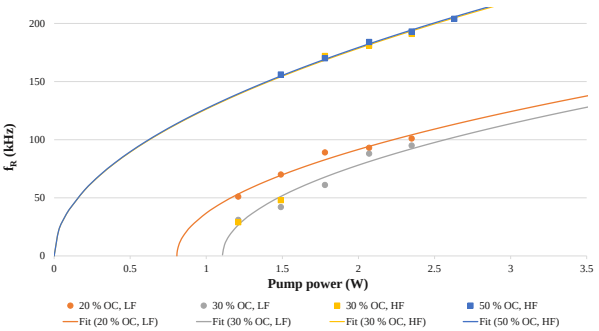

Figure 12: Pulse repetition frequency with the SAM-3000, for different output couplers. The lines show the fittings with model function $f_R = a\sqrt{P_{\text{pump}} - P_{\text{th}}}$.

Figure 12 shows the pulse repetition frequency of the pulses for different output couplers when the SAM-3000 is used. The 30 % output coupler setup was characterised for two different positions of the SESAM, obtaining different Q-switching operation regimes.

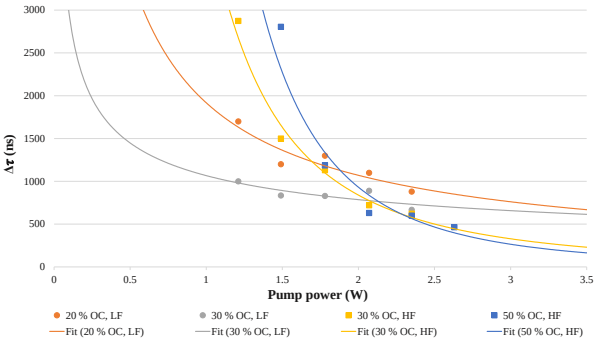

Figure 13: Full width at half maximum $\Delta\tau$ with the SAM-3000, for different output couplers. The lines represent the fittings with model function $\Delta\tau = a P_{\text{pump}}^{-b}$.

Figure 13 shows, instead, the full width at half maximum of the pulses. For a given pump power, to a higher repetition frequency corresponds a shorter lifetime of the single pulse inside the cavity and, accordingly, a lower amplification. Because of the lower pulse power, the saturable absorption effect decreases, increasing the pulse width. The modulation depth of any saturable absorber is however limited, therefore for high enough pump powers the performance of the device does not change considerably between frequency regimes. When the transmission of the output coupler is increased, instead, the pulses have a shorter full width at half maximum, since the increased losses make the radiation in the cavity discharge faster.

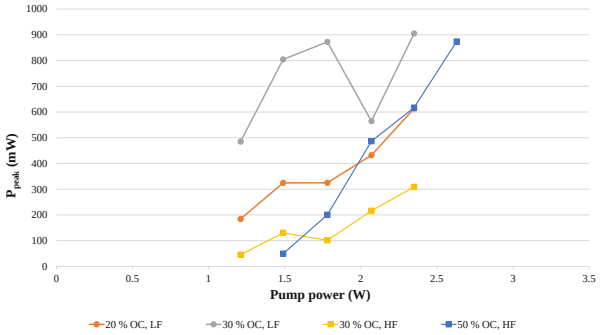

Figure 14: Peak pulse power P_{peak} with the SESAM-3000, for different output couplers.

Lastly, Figure 14 shows the computed peak pulse power. We notice that the 30 % output coupler setup in the lower frequency regime has the highest peak pulse power. The corresponding higher repetition frequency regime has instead much lower peak powers, since the shorter lifetime of the single pulse in the cavity reduces its energy. Moreover, the lower pulse power reduces absorption saturation, increasing the losses and further lowering the peak power.
Similar measurements were taken with another semiconductor saturable absorber, the SAM-2900, obtaining a similar performance. An interesting regime was observed, for high enough pump powers, with a $T = 50\,\%$ output coupler: we measured short pulses with simultaneously high average power and low repetition frequency, thus high peak powers, up to 3069 mW.
The same measurements were performed substituting the SESAM with a protected gold mirror, whose coating shows saturable absorption,

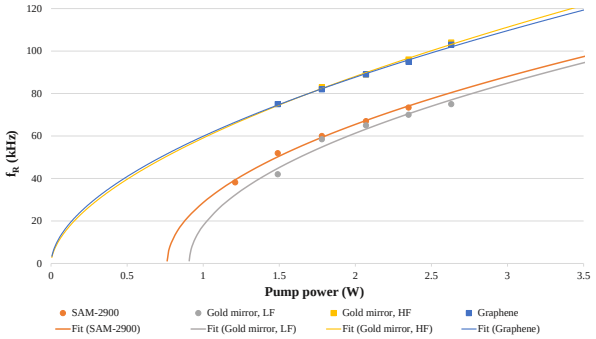

Figure 15: Pulse repetition frequency with different saturable absorber mirrors and a 10 % output coupler. The lines represent the fittings with model function $f_R = a\sqrt{P_{\text{pump}} - b}$.

and with a mid-infrared enhanced gold mirror, obtaining stable Q-switching in both cases. Figure 15 compares the repetition frequency with different saturable absorber mirrors. Overall, we can clearly identify two regimes, characterised by different frequencies.

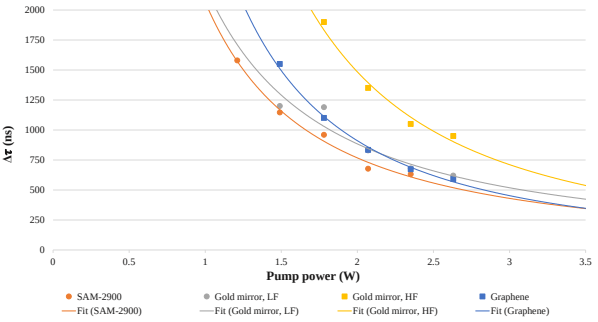

Figure 16: Full width at half maximum for different saturable absorber mirrors, with a 10 % output coupler. The lines represent the fittings with model function $\Delta\tau = aP_{\text{pump}}^{-b}$.

Figure 16 shows, instead, the full width at half maximum of the pulses for different saturable absorber mirrors. We see that the SAM-2900 and the gold mirror give comparable performances when operating in regimes with similar repetition frequency. The higher frequency gold mirror measurements, instead, correspond to visibly broader pulses, because of the lower absorption saturation. Finally, we notice that graphene, even though it corresponds to a higher repetition frequency, generates pulses with a time duration comparable to the one of lower frequency pulses.

3. Conclusions and future developments

In this thesis work we have investigated the laser performance of an in-band pumped Dy-doped fluorozirconate fibre emitting around 3 µm. In a continuous wave configuration we have obtained a maximum laser output power of 248 mW and a maximum slope efficiency of 44 %. Investigating pulsed laser operation, we have tested different saturable absorbers, demonstrating stable passive Q-switching operation with a minimum pulse duration of 464 ns, a highest repetition frequency of 210 kHz and peak pulse powers up to 3069 mW.

These results are promising for the generation of ultrashort pulses in the 3 µm spectral region. Indeed, starting from the experimental results obtained in the Q-switching regime we have been able to identify some steps which could bring the laser in passive mode-locking regime. Namely, the gain of the laser cavity must be increased, by employing a longer fibre or by increasing the maximum injected power, and higher-performing saturable absorbers must be employed. These results will open the way for the synthesis of novel fibre frequency combs in the mid-infrared spectral region around 3 µm, which in recent years have been revolutionising the field of high-precision broadband spectroscopy.

4. Acknowledgements

I would like to thank my thesis advisors Prof. Paolo Laporta from Politecnico di Milano and Dr. Gianluca Galzerano from CNR-IFN. I would also like to give thanks to Yuchen Wang, Lisa Molteni and Prof. Pinghua Tang from Xiangtan University.

References

[1] Orazio Svelto. *Principles of lasers*. 5. ed. Springer, 2010. XXI, 620. ISBN: 9781441913012.

[2] Yuchen Wang et al. "Ultrafast Dy^{3+}:fluoride fiber laser beyond 3 µm". In: *Opt. Lett.* 44.2 (Jan. 2019), pp. 395–398. DOI: 10.1364/OL.44.000395.

[3] Yuchen Wang et al. "Mid-IR tunable CW and passively Q-switched laser operation of Dy-doped fluoride fiber". In: *Opt. Mater. Express* 12.4 (Apr. 2022), pp. 1502–1511. DOI: 10.1364/OME.453046.

[4] Stuart D. Jackson. "Towards high-power mid-infrared emission from a fibre laser". In: *Nature Photonics* 6.7 (2012), pp. 423–431. ISSN: 1749-4893. DOI: 10.1038/nphoton.2012.149.